

# Supplementary Information for

## **Thermal effects - an alternative mechanism for plasmonic-assisted photo-catalysis**

Yonatan Dubi,<sup>1,4</sup> Ieng Wai Un,<sup>2,3</sup> Yonatan Sivan<sup>2,4\*</sup>

<sup>1</sup>Department of Chemistry, Ben-Gurion University, Israel

<sup>2</sup>School of Electrical and Computer Engineering, Ben-Gurion University, Israel

<sup>3</sup>Joan and Irwin Jacobs TIX Institute, National Tsing Hua University, Taiwan

<sup>4</sup> Ilse Katz Center for Nanoscale Science and Technology, Ben-Gurion University, Israel

\*To whom correspondence should be addressed; E-mail: jdubi@bgu.ac.il

(Dated: April 28, 2020)

## I. ARRHENIUS ANALYSIS OF PAPER II

Unfortunately, Paper II does not supply data for the reaction rate as a function of temperature, neither in the dark nor under illumination. Therefore, a direct Arrhenius analysis in similarity to the one performed for Paper I (see our Fig. 2 in the main text) is impossible. Yet, Paper II does supply one plot (Fig. 3a) which can be used to test our thermal approach. This plot shows the reaction rate as a function of illumination intensity under constant measured temperature  $T_M = 100^\circ\text{C}$  (i.e., when the external heater temperature and the illumination intensity are changed simultaneously to maintain  $T_M$ ). Assuming again that the temperature felt by the catalytic sites is  $T = T_M + \tilde{a}I_{inc}$  (Eq. (3)), we fit the data of Fig. 3a to an Arrhenius curve  $R = R_0 \exp\left(\frac{\mathcal{E}_a}{T_M + \tilde{a}I_{inc}}\right)$ , allowing  $R_0$ , as well as  $\mathcal{E}_a$  and  $\tilde{a}$  to vary. The data and the fitted Arrhenius curve are shown in Fig. S1. One can observe a remarkable match to the data of Paper II, with the fit parameters  $\mathcal{E}_a = 0.2\text{eV}$  and  $\tilde{a} = 421\text{Kcm}^2/\text{W}$ . Notice especially the excellent agreement between data and fit at the low intensity side, which is completely missed in the fit originally offered in Fig. 3a of Paper II. Remarkably, the activation energy is very close to the one we find from the data of Paper I, and much smaller than the reported one. The photothermal conversion coefficient  $\tilde{a}$  is, however, about 10 – 12 times larger than that found from the data of Paper I. In the absence of a detailed description of the host in Paper II (nor in Paper I), we are bound to make a single simple assumption - that the host has a significant content of oxide. Under this condition, the thermal conductivity of the host is dominated by the oxide, and the detailed calculations in Supplementary Section II below imply that the temperature rise of the sample is inversely proportional to the thermal conductivity of the oxide. Thus, since the thermal conductivity of  $\text{SiO}_2$  is several times smaller than of  $\text{TiO}_2$ , the photothermal conversion coefficient of the sample in Paper II is indeed expected to be much higher than in Paper I, in agreement with the fit results above.

## II. DETAILED TEMPERATURE CALCULATIONS

In this Supplementary Information Section, we compute the temperature of the catalyst pellet described in [1, Paper III] and [2, Paper IV], respectively. We describe in detail the assumptions employed in the calculations, the calculation procedure itself, and discuss the

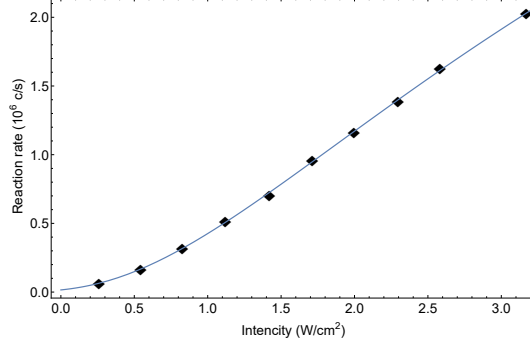


FIG. S1. (Color online) reaction rate as a function of illumination intensity, data from Paper II. Solid line is a fit to an Arrhenius curve, yielding the fit parameters  $\mathcal{E}_a = 0.2\text{eV}$  and  $\tilde{a} = 421\text{ K cm}^2/\text{W}$ .

sensitivity of the results to the uncertainty in the various parameters.

### A. Detailed temperature calculations for Paper III

In [1, Paper III], the catalyst pellet consisted of Ag nanocubes (edge length 75 nm) mixed with larger  $\text{Al}_2\text{O}_3$  particles. For simplicity, we approximate the system as a (periodic) Ag NP array immersed in a uniform host material. Specifically, the nanocubes are approximated by nanospheres of radius  $R = 55\text{ nm}$  such that the volume of the cubes and spheres are approximately the same. Based on the reported concentration of Ag (20 wt%) in the composite [1, Paper III] and the reported size of the catalyst layer [3] (thickness  $H = 0.5\text{ mm}$ ) [4], we can estimate that the average separation between Ag particles is  $p \approx 354\text{ nm}$ .

For the host material, we set the (effective) permittivity to be  $\varepsilon_h = (1 - f_v)\varepsilon_{\text{air}} + f_v\varepsilon_{\text{Al}_2\text{O}_3}$  and the thermal conductivity to be [5–7]

$$\kappa_h = \kappa_{\text{air}} + \frac{3f_v\kappa_{\text{air}}}{\frac{\kappa_{\text{Al}_2\text{O}_3} + 2\kappa_{\text{air}}}{\kappa_{\text{Al}_2\text{O}_3} - \kappa_{\text{air}}} - f_v}, \quad (\text{S1})$$

where  $f_v$  is the volume fraction of oxide in the composite (estimated from the data to be  $\sim 10\%$ ). This relatively advanced effective medium formula used for the thermal conductivity is required due to the large differences between the thermal conductivities of the constituents. Physically, it shows that the air serves as the bottle neck for heat conduction in the system.

The settings for the nanosphere radius and the fraction of  $\varepsilon_{\text{Al}_2\text{O}_3}$  in  $\varepsilon_h$  are verified by comparing the calculated extinction cross-section with the measured extinction spectrum [1,

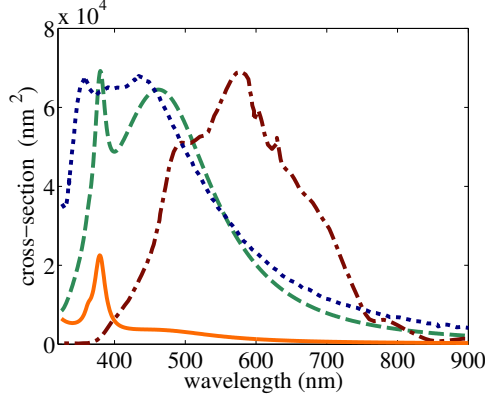


FIG. S2. (Color online) Calculated extinction (green dashed line) and absorption (orange solid line) cross-section of an Ag nanosphere of 55 nm in radius at temperature 373 K using the high temperature ellipsometry data of [8]. The measured extinction spectrum of Ag nanocube (blue dotted line) and the emission spectrum of the visible light source (red dashed-dotted line)  $i_{\text{inc}}(\omega)$  are also shown.

Paper III], as shown in Fig. S2. One can see that the differences in the extinction between the calculation and measurement are mostly in the region which the light source has a low spectral density.

The sample is subject to white light continuous wave (CW) illumination. The spectrum of the CW light source (copied from reference [1, Paper III])  $i_{\text{inc}}(\omega)$  is shown in Fig. S2 and the incident intensity is  $I_{\text{inc}} = \int i_{\text{inc}}(\omega) d\omega$  with a spot size of  $A \sim 1 \text{ cm}^2$  ( $\sim 5.6 \text{ mm}$  in radius) which is assumed to be similar to the area of the quartz window of the reaction chamber.

The temperature distribution in the catalyst pellet  $T(\mathbf{r})$  can be obtained by solving the heat equation

$$\begin{cases} \nabla \cdot [\kappa_m \nabla T(\mathbf{r})] = -p_{\text{abs}}(\mathbf{r}), & \text{for } \mathbf{r} \text{ in NPs,} \\ \nabla \cdot [\kappa_h \nabla T(\mathbf{r})] = 0, & \text{for } \mathbf{r} \text{ in host,} \end{cases} \quad (\text{S2})$$

with appropriate boundary conditions at the surface of each NP [9]. Here,  $p_{\text{abs}}(\mathbf{r})$  is the absorbed power density; it is related to the total (local) electric field  $\mathbf{E}(\omega, \mathbf{r})$  via  $p_{\text{abs}}(\mathbf{r}) = \int \frac{\omega}{2} \varepsilon_m''(\omega, \mathbf{r}) |\mathbf{E}(\omega, \mathbf{r})|^2 d\omega$  [10]. At room temperature, the total (local) electric field and, thus, the absorbed power density can be obtained just by solving the Maxwell's equations. However, due to the large domain size and the huge number ( $10^{12}$ ) of NPs, such

numerical calculation could be time-consuming or even unfeasible.

To simplify the problem, we neglect the temperature dependence of the permittivities and the thermal conductivities; this will be justified a-posteriori by the modest temperature rise of only a few tens of degrees that shall be retrieved. Further, since  $R \ll p < \lambda$ , i.e., since the particle density is relatively low, we can apply the effective medium approximation such that we can write the incident field intensity as  $i(\mathbf{r}, \omega) = i_{\text{inc}}(\omega) \exp(-z/\delta_{\text{skin}}(\omega))$  due to the absorption by the NPs, where  $1/\delta_{\text{skin}}$  is the absorption coefficient experienced by the incident beam; the transverse profile of the illumination is assumed to be uniform.

The absorption coefficient can be obtained by considering the change of spectral intensity per unit length along the propagation direction, namely,

$$\frac{\Delta i(\omega, z)}{\Delta z} = -\frac{i(\omega, z)\sigma_{\text{abs}}(\omega)A/p^2}{A} \frac{1}{p} = -i(\omega, z)\frac{\sigma_{\text{abs}}(\omega)}{p^3},$$

where  $\Delta z \sim p$  is the thickness of one layer,  $i(\omega, z)\sigma_{\text{abs}}(\omega)$  is the absorbed power per unit frequency per NP and  $A/p^2$  is the number of NPs per layer, so  $i(\omega, z)\sigma_{\text{abs}}(\omega)A/p^2$  is the total absorbed power per unit frequency; we divide it by  $A$  to obtain the intensity loss per unit frequency. Then, the penetration (or, skin) depth of light into the sample is

$$\delta_{\text{skin}}(\omega) \approx p^3/\sigma_{\text{abs}}(\omega). \quad (\text{S3})$$

For visible wavelengths, the skin depth ranges from 15  $\mu\text{m}$  to 100  $\mu\text{m}$ .

Since  $\kappa_m \gg \kappa_h$ , the temperature is uniform within each NP even if  $p_{\text{abs}}(\mathbf{r})$  is highly non-uniform [9, 11]. This further allows us to replace the spatial-dependent  $p_{\text{abs}}(\mathbf{r})$  in each NP by its spatial average over the NP at  $\mathbf{r}_i$ , namely,

$$\begin{aligned} \bar{p}_{\text{abs},i} &= \frac{1}{V_{\text{NP}}} \int_{V_{\text{NP},i}} p_{\text{abs}}(\mathbf{r}) d^3r = \frac{1}{V_{\text{NP}}} \int \int_{V_{\text{NP},i}} \frac{\omega}{2} \varepsilon_m'' |\mathbf{E}(\omega, \mathbf{r})|^2 d^3r d\omega \\ &= \frac{1}{V_{\text{NP}}} \int i_{\text{inc}}(\omega) e^{-z_i/\delta_{\text{skin}}(\omega)} \sigma_{\text{abs}}(\omega) d\omega, \end{aligned} \quad (\text{S4})$$

where

$$\int_{V_{\text{NP},i}} \frac{\omega}{2} \varepsilon_m'' |\mathbf{E}(\omega, \mathbf{r})|^2 d^3r = i_{\text{inc}}(\omega) e^{-z_i/\delta_{\text{skin}}(\omega)} \sigma_{\text{abs}}(\omega).$$

Furthermore, since the heat equation (S2) is a linear differential equation, the temperature  $T(\mathbf{r})$  in the multiple NP problem can be written as the linear combination of all the *single* NP contribution to the temperature rise (denoted by  $\Delta T_i(\mathbf{r})$ ) under CW illumination [12],

namely,

$$\Delta T_i(\mathbf{r}) = \frac{V_{\text{NP}} \bar{p}_{\text{abs},i}}{4\pi\kappa_h} \begin{cases} 1/R, & \text{for } |\mathbf{r} - \mathbf{r}_i| < R, \\ 1/|\mathbf{r} - \mathbf{r}_i| & \text{for } |\mathbf{r} - \mathbf{r}_i| > R. \end{cases} \quad (\text{S5})$$

Here, the symbol  $\Delta$  denotes the difference with respect to the temperature in the absence of illumination,  $T_{\text{dark}}$ . Then, the solution for the multiple NP problem is

$$\Delta T(\mathbf{r}) = \begin{cases} \frac{V_{\text{NP}}}{4\pi\kappa_h} \left[ \frac{\bar{p}_{\text{abs},i}}{R} + \sum_{j \neq i} \frac{\bar{p}_{\text{abs},j}}{|\mathbf{r}_j - \mathbf{r}_i|} \right], & \text{for NP at } \mathbf{r}_i, \\ \frac{V_{\text{NP}}}{4\pi\kappa_h} \sum_j \frac{\bar{p}_{\text{abs},j}}{|\mathbf{r}_j - \mathbf{r}|}, & \text{for } \mathbf{r} \text{ in the host.} \end{cases} \quad (\text{S6})$$

The summation can be converted into an equivalent integration by dividing by the NP density [12], namely,

$$\sum_{j \neq i} \frac{e^{-z_j/\delta_{\text{skin}}}}{|\mathbf{r}_j - \mathbf{r}_i|} \rightarrow \frac{1}{p^3} \int_{V'_{\text{composite}}} \frac{e^{-z'/\delta_{\text{skin}}}}{|\mathbf{r}' - \mathbf{r}_i|} d^3r', \quad (\text{S7})$$

where  $V'_{\text{composite}}$  denotes the composite volume under the illumination but without the unit cell at  $\mathbf{r}_i$ .

Once the temperature is determined, one can define the photo-thermal conversion coefficient  $a$ , namely,

$$a = \frac{\langle \Delta T \rangle_{\text{top surface}}}{\int i_{\text{inc}}(\omega) d\omega}, \quad (\text{S8})$$

where  $\langle \Delta T \rangle_{\text{top surface}} = \int_{\text{top surface}} \Delta T(\mathbf{r}) \rho d\rho d\phi / A$  is the average temperature over the top surface of the pellet [13].

We first calculate the absorption cross-section of a single NP by using the Ag permittivity from the reference [8] and Mie theory; the result is shown in Fig. S2. One can see that the scattering dominates absorption; a quadrupole resonance is seen at  $\lambda \sim 380$  nm and a broad dipole resonance is seen at  $\lambda \sim 480$  nm. The latter dominates the particle absorption since it overlaps with the spectrum of the CW light source much better than the quadrupole resonance.

Then, the temperature profile on the top surface of the pellet can be obtained by Eq. (S6), see Fig. S3. One can see that the temperature of the top surface decreases gradually from 492 K at the center ( $\rho = 0, z = 0$ ) to 461 K at the edges ( $\rho = D/2, z = 0$ ). Thus, the

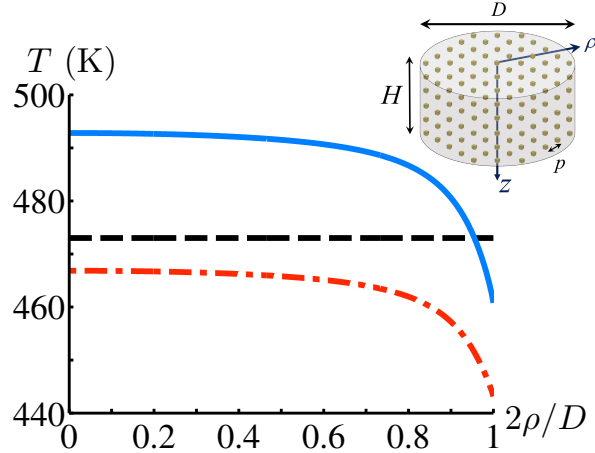


FIG. S3. (Color online) Temperature at the top surface ( $z = 0$ ) of the pellet in the dark (red dash-dotted line), and under CW illumination of intensity  $0.4 \text{ W/cm}^2$  (blue solid line). In both cases, the temperature at the bottom of the pellet is fixed to 473 K, i.e. the measured temperature (black dashed line).  $\rho$  is the radius coordinate and  $D$  is the diameter of the pellet, as shown in the inset.

overall composite temperature rise is, in fact, a many-particle effect, much higher than the temperature rise (4.3 mK) of a single-particle model used in reference [1, Paper III] and reference [3]. The temperature at the center is higher just because the heat arrives from all directions, whereas in the periphery, it arrives only from the center of the pellet. After averaging the surface temperature, Eq. (S8) gives  $a = 40 \text{ K cm}^2/\text{W}$ . This value is similar to the value obtained for  $\tilde{a}$  from the shifted Arrhenius Law in Section III B (Fig. 3).

A comparison of the temperatures of the top and bottom interfaces of the pellet also reveals a vertical temperature gradient. In the thermocatalysis control experiment, the gradient is negative (top is cooler; here, by 7K for a heater set to 473K) and in the photocatalysis experiment, the gradient is positive (top is hotter; by 16K for the same condition). These intuitive results were confirmed in [14]. They also imply that the thermocouple was positioned right at the bottom of the pellet (information which is not provided in III, but confirmed in private communications).

One should bear in mind that the value we obtained for  $a$  should be considered only as an order-of-magnitude estimate. Indeed, as mentioned above, the beam size is not specified in Paper III. For example, if the beam radius is changed from 5.6 mm to 2.8 mm, the

maximum composite temperature rise changes from 16 K to 7.7 K for a fixed illumination intensity of  $0.4 \text{ W/cm}^2$  (not shown). The value for  $a$  would also depend on the inter-particle separation. Specifically, larger inter-particle separation may lead to a decrease in the composite temperature. However, this will also cause an increase in the skin depth (see Eq. (S3)), hence to broadening of the heat source. Yet, since the skin depth in [1, Paper III] is much smaller than the thickness of the pellet, still all the incident photon energy is absorbed.

In addition, one might expect that the approximation of the nanocube by a nanosphere will yield a somewhat different value for the conversion factor  $a$  due to the difference in the respective absorption cross-sections. However, similarly, an increase of  $\sigma_{\text{abs}}$  also causes a decrease of skin depth (see Eq. (S3)) such that the composite temperature rise is also weakly sensitive to the particle shape.

## B. Detailed temperature calculations for Paper IV

The catalyst pellet in [2, Paper IV] consisted of Cu-Ru NPs of radius 2.5 nm supported on larger porous  $\text{Al}_2\text{O}_3$ -MgO particles. We approximate the system as a Cu-Ru nanosphere (periodic) array immersed in a uniform host material. Under these assumptions, one can deduce from the measurements of the Cu concentration reported in reference [2, Paper IV] that the average inter-particle separation is  $p = 24.5 \text{ nm}$ . Further, the optical properties of the metal NPs are characterized by  $\varepsilon_m = 0.99\varepsilon_{\text{Cu}} + 0.01\varepsilon_{\text{Ru}}$  [15] according to the element concentration measurements in [2, Paper IV]; since the thermal properties are similar for Cu and Ru, they are assumed simply to be  $c_m = c_{\text{Cu}}$ ,  $\rho_m = \rho_{\text{Cu}}$  and  $\kappa_m = \kappa_{\text{Cu}}$ .

For the host material, we set the host permittivity to be  $\varepsilon_h = (1 - f_v)\varepsilon_{\text{air}} + 0.5f_v\varepsilon_{\text{Al}_2\text{O}_3} + 0.5f_v\varepsilon_{\text{MgO}}$ , the host volumetric heat capacity to be  $\rho_h c_h = (1 - f_v)\rho_{\text{air}}c_{\text{air}} + 0.5f_v\rho_{\text{Al}_2\text{O}_3}c_{\text{Al}_2\text{O}_3} + 0.5f_v\rho_{\text{MgO}}c_{\text{MgO}}$  and the thermal conductivity of the host to be [6, 7]

$$\kappa_h = \kappa_{\text{air}} + \frac{3f_v\kappa_{\text{air}}}{\frac{(\kappa_{\text{Al}_2\text{O}_3} + \kappa_{\text{MgO}})/2 + 2\kappa_{\text{air}}}{(\kappa_{\text{Al}_2\text{O}_3} + \kappa_{\text{MgO}})/2 - \kappa_{\text{air}}} - f_v}, \quad (\text{S9})$$

where  $f_v$  is the volume fraction of oxides in the composite which can be deduced from the mass (1.1 mg) and the volume (diameter  $D = 2 \text{ mm}$  and thickness  $H = 1 \text{ mm}$ ) of the pellet [2]. As in Supplementary Section II A, the relatively more advanced effective medium formula used for the thermal conductivity is required due to the large differences between

the conductivities of the constituents. This choice for the various filling factors is confirmed by comparing the calculated absorption cross-section  $\sigma_{\text{abs}}$  shown in Fig. S4 with the diffusive reflection measurement shown in the supplementary information of reference [2, Paper IV].

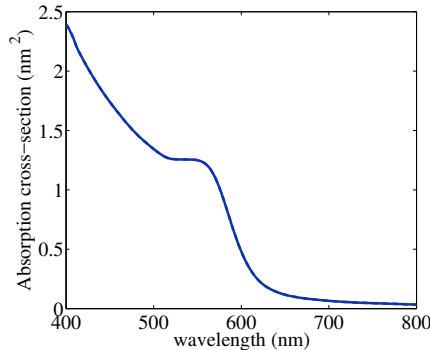


FIG. S4. (Color online) Calculated absorption cross-section of Cu-Ru NP ( $\epsilon_m = 0.99\epsilon_{\text{Cu}} + 0.01\epsilon_{\text{Ru}}$ ) in a uniform host ( $\epsilon_h = 0.9\epsilon_{\text{air}} + 0.05\epsilon_{\text{Al}_2\text{O}_3} + 0.05\epsilon_{\text{MgO}}$ ).

The pulse train illumination on the pellet is set below to have a (time) average incident intensity  $\langle I_{\text{inc}} \rangle = 4 \text{ W/cm}^2$  with central wavelength 550 nm (as in Fig. 5(A) in Section III C), spot size  $A = \pi \cdot 1 \text{ mm}^2 \sim D^2$ , average power  $\langle P_{\text{inc}} \rangle = \langle I_{\text{inc}} \rangle A$ , pulse repetition rate  $f = 80 \text{ MHz}$  (i.e., pulse period  $\sim 12.5 \text{ ns}$ ) and pulse duration  $\tau = 4 \text{ ps}$ . The energy per pulse is thus  $\langle P_{\text{inc}} \rangle / f$ , and the peak pulse intensity is  $I_{\text{max}} = \langle P_{\text{inc}} \rangle / (A \cdot f \cdot \tau) = \langle I_{\text{inc}} \rangle / (f \cdot \tau)$ .

### 1. Temperature dynamics of the composite - formulation

The spatio-temporal evolution of the catalyst temperature,  $T(\mathbf{r}, t)$ , can be determined by solving the heat equation,

$$\begin{cases} \rho_m c_m \frac{\partial T(\mathbf{r}, t)}{\partial t} - \kappa_m \nabla^2 T(\mathbf{r}, t) = p_{\text{abs}}(\mathbf{r}, t), & \text{for } \mathbf{r} \text{ in NPs,} \\ \rho_h c_h \frac{\partial T(\mathbf{r}, t)}{\partial t} - \kappa_h \nabla^2 T(\mathbf{r}, t) = 0, & \text{for } \mathbf{r} \text{ in the host,} \end{cases} \quad (\text{S10})$$

with appropriate boundary conditions at the surface of each NP [16]. For simplicity (as in Supplementary Section II A), we ignore the temperature dependence of  $\kappa_h$ ,  $c_h$  and  $\rho_h$ . This dependence should be included for sufficiently high temperatures, typically, for  $T > 400 \text{ K}$  forcing one to solve Maxwell's equations together with the heat equation (S2) self-consistently [17, 18]. This is motivated by the weak sensitivity of the pellet temperature

distribution to the inter-particle separation and absorptivity, as discussed in Supplementary Section II A.

As in Supplementary Section II A, due to the absorption by the NPs, the peak pulse intensity drops along the thickness of the pellet. Since  $R \ll p \ll \lambda$  and absorption dominates scattering for NP size of a few nm, we can apply the effective medium approximation such that the spatial dependence of the peak pulse intensity can be written as  $I_{\max} \exp(-z/\delta_{\text{skin}})$ . The penetration (skin) depth is estimated by

$$\delta_{\text{skin}} = p^3/\sigma_{\text{abs}} \sim 12 \mu\text{m}, \quad (\text{S11})$$

a value which is similar to that (10  $\mu\text{m}$ ) provided in the supplementary of reference [2, Paper IV].

Since the heat equation is a linear differential equation, the problem can be simplified by first looking for the temperature evolution of a *single* NP at  $\mathbf{r} = 0$  under a *single* pulse illumination at  $t = 0$ , denoted by  $\Delta T_{0,0}(\mathbf{r}, t)$ , namely,

$$\begin{cases} \rho_m c_m \frac{\partial T_{0,0}(\mathbf{r}, t)}{\partial t} - \kappa_m \nabla^2 T_{0,0}(\mathbf{r}, t) = p_{\text{abs},0,0}(\mathbf{r}, t), & \text{for } r < R, \\ \rho_h c_h \frac{\partial T_{0,0}(\mathbf{r}, t)}{\partial t} - \kappa_h \nabla^2 T_{0,0}(\mathbf{r}, t) = 0, & \text{for } r > R, \end{cases} \quad (\text{S12})$$

with appropriate boundary conditions at  $r = R$  [16], and where  $p_{\text{abs},0,0}(\mathbf{r}, t)$  is the absorbed power density under a *single* pulse illumination, the integration of which over space-time is the total energy absorbed per pulse by a *single* NP,  $\int \int p_{\text{abs},0,0}(\mathbf{r}, t) d\mathbf{r} dt = \mathcal{E}_0 = \sigma_{\text{abs}} \langle I_{\text{inc}} \rangle / f$ . Then, the solution for the pulse train illumination of the multiple particle composite can be obtained by the linear combination of many solutions of *single* pulse events from all particles, namely,

$$\Delta T(\mathbf{r}, t) = \sum_{t_k < t} \sum_j \Delta T_{0,0}(\mathbf{r} - \mathbf{r}_j, t - t_k) \exp(-z_j/\delta_{\text{skin}}), \quad (\text{S13})$$

where  $t_k = k/f$  is the pulse time,  $k = 0, 1, \dots$ . Eventually, the system reaches a “steady-state” (see Fig. S5(B)), as shown below, in which case the photo-thermal conversion coefficient can be defined by

$$a = \frac{\langle \Delta T(t \rightarrow \infty) \rangle_{\text{top surface}}}{\langle I_{\text{inc}} \rangle}, \quad (\text{S14})$$

where  $\langle \Delta T(t \rightarrow \infty) \rangle_{\text{top surface}}$  stands for the average temperature on the top surface of the pellet in the “steady-state”.

In what follows, we discuss these calculation steps separately.

## 2. Single particle temperature $\Delta T_{0,0}$

The spatio-temporal evolution of the NP temperature is a result of a series of processes:

1. the inner temperature rise dynamics within the NP (due to photon absorption) occurring on a time scale of the pulse duration  $\tau$ , and resulting in an increase of inner temperature by  $\mathcal{E}_0/\rho_m c_m V_{\text{NP}} \approx 1.8$  mK,
2. the inner NP temperature decay due to heat transfer to the host, estimated to occur within  $\tau_{\text{NP}}^{\text{d}} \equiv R^2 \rho_m c_m / 3\kappa_h \sim 0.2$  ns [16] and
3. heat diffusion in the host, occurring on a much longer time scale.

Since we are interested only in the long time dynamics (specifically, the “steady-state” of the composite temperature) for the purpose of the photocatalysis experiments and since  $\tau \ll \tau_{\text{NP}}^{\text{d}} \ll 1/f$ , we can treat these stages separately without compromising the accuracy. Furthermore, the heat equation (S12) can be simplified by approximating the NP as a point-source such that the absorbed power density is represented by a space-time Dirac delta distribution [16],

$$\rho_h c_h \frac{\partial T_{0,0}(\mathbf{r}, t)}{\partial t} = \kappa_h \nabla^2 T_{0,0}(\mathbf{r}, t) + \mathcal{E}_0 \delta(\mathbf{r}) \delta(t). \quad (\text{S15})$$

Eq. (S15) has the analytic solution

$$\Delta T_{0,0}(\mathbf{r}, t) = \frac{\mathcal{E}_0}{\rho_h c_h} \frac{1}{(4\pi d_h t)^{3/2}} \exp\left(-\frac{r^2}{4d_h t}\right), \quad (\text{S16})$$

where  $d_h = \kappa_h/(\rho_h c_h)$  is the diffusivity of the host.

## 3. The steady-state temperature and temperature uniformity under pulse train illumination

In order to understand the temperature evolution under *pulse train* illumination, we first study the temperature evolution of the NP at the top center of the pellet for a *single* pulse illumination, see Fig. S5(A). One can see that most of the absorbed energy leaves the NP and diffuses in the host so that the inner temperature decays within the first 2 ns. Then, the NP temperature increases due to the heat diffusion from the (many) other NPs, such that this heat diffusion keeps the NP warm at 0.25 mK for more than 50 ms. Eventually, the NP temperature decays again to zero when all the thermal energy diffuses out of the pellet.

Then, the temperature evolution under *pulse train* illumination can be obtained by a summation of many (time-shifted) *single* pulse events. Since the pulse repetition rate is faster than the overall decay time to the environment, there is an overall (“step-wise”)

temperature buildup under *pulse train* illumination, see Fig. S5(B). This heat accumulation finally slows down and the temperature reaches a “steady-state” of  $\Delta T \sim 680$  K on a time scale of a few seconds, as shown in Fig. S5(B). One can also calculate the “steady-state” temperature profile on the top surface of the pellet, see Fig. S6(B). The photo-thermal conversion coefficient is deduced to be  $\sim 170$  K cm<sup>2</sup>/W in Section III C.

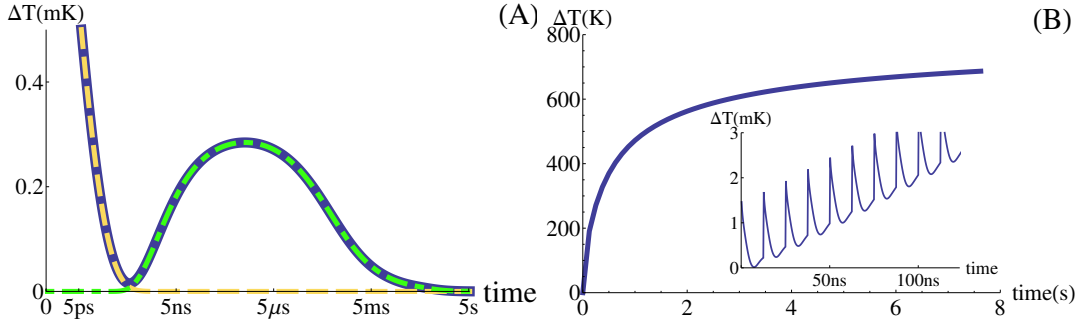


FIG. S5. (Color online) (A) Temperature evolution at the top center of the pellet under a *single* pulse illumination (blue solid line), the contribution from the inner temperature rise (yellow dashed line) and the heat diffusion from (many) other NPs (green dash-dotted line) are also shown. Note that the time axis is not a linear scale. (B) Temperature evolution at the top center of the pellet under *pulse train* illumination. The insert shows the temperature evolution during the illumination of the first several pulses, the time axis is similar to that in (B).

Similar to the analysis in Supplementary Section II A, the “steady-state” temperature is weakly sensitive to the inter-particle separation (within the parameter range deduced from the SEM pictures) due to the opposite effect of the particle density and the skin depth on the “steady-state” temperature. We should note that our calculations assumed for simplicity that the chamber in which the pellet is held has infinite size. In practice, the actual pellet temperature could be partially reduced by a few ten percents because the temperature of the chamber walls was maintained at 300 K in the experiment [2]. Due to all the above, overall, the value obtained for the photo-thermal conversion coefficient should be viewed as an order-of-magnitude estimate.

Having said the above, we should emphasize that the most important aspect of our calculation is qualitative, as it shows the significant temperature gradients across the pellet. Indeed, since only the NPs in the pellet surface layer of thickness ( $\sim \delta_{\text{skin}}$ ) generate heat under illumination, large temperature non-uniformity would be expected across the pellet.

By using Eqs. (S13) and (S16), we can calculate the “steady-state” temperature profile along the cylindrical axis and along the radial direction on the top surface of the pellet, see Figs. S6(A) and (B), respectively. One can see that the temperature gradually decreases from 680 K to 250 K along the cylindrical axis. In the transverse direction, the non-uniformity is somewhat smaller. As explained in Section IV (and [19]), these non-uniformities cause severe differences between the thermal contributions in the photocatalysis and thermocatalysis control experiments, thus, invalidating the conclusions of [2].

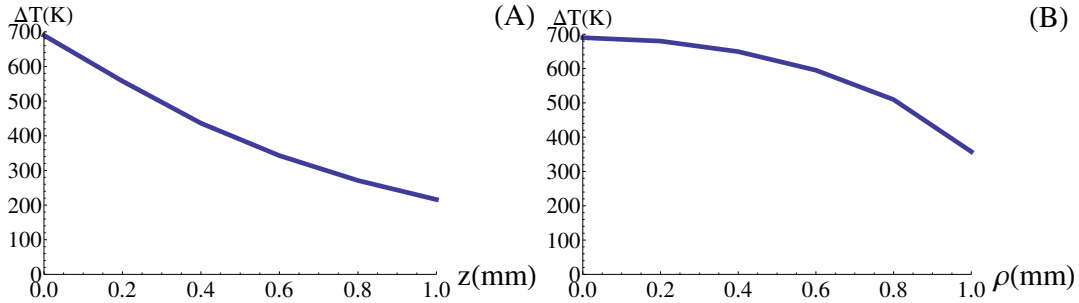


FIG. S6. (Color online) Temperature rise profile (A) along the cylindrical axis of the pullet and (B) along the radial direction on the top surface of the pellet.

### III. A THERMAL MODEL FOR THE DATA OF REF. [3]

In Ref. [3] an increase in reaction rates under illumination is reported (Figs. 1b and 3a), which is claimed to be impossible to be fitted using a thermal theory of an Arrhenius form. However, this is incorrect, and the reason the authors failed to fit their data with an Arrhenius plot, is that they limited the fitting temperature rise to be in the milliKelvin range, motivated by their (single-particle) calculations. However, as some of the authors later report, in a similar system, a surface temperature rise of a few degrees K was observed [20].

We have repeated the fitting procedure described in the main text, using the data from [3]) (extracted digitally). In the left panel of Fig. S7, the black triangles are the reaction rate in the dark, from which an activation energy was extracted ( $\mathcal{E}_a = 0.88\text{eV}$ ). The solid dark line is an Arrhenius plot of the reaction rate with the  $\mathcal{E}_a$  extracted above. Using this activation energy, a temperature shift  $\Delta T$  was extracted from the reaction rate under illumination of intensity  $I_{inc} = 250\text{mW cm}^{-2}$ . We find a temperature increase of  $\Delta T \sim 20\text{K}$ , somewhat larger than in [3] (keep in mind that these are different experiments, and the temperature

increase can be highly sensitive to the experimental details and the physical properties of the catalytic pellet etc.). The red solid line shows the fit to the shifted Arrhenius form.

From the shift in temperature at a given intensity, we can find the photothermal conversion coefficient,  $\tilde{a} = \Delta T/I_{inc}$ , which is found to be  $\tilde{a} = 80\text{K cm}^2/\text{W}$ . Using this coefficient, we can now plot the reaction rate as a function of intensity, with essentially no fitting parameters (except for the overall coefficient). This is shown as the solid line in the right panel of Fig. S7, placed on top of the experimental data. The excellent correspondence between the two is evident.

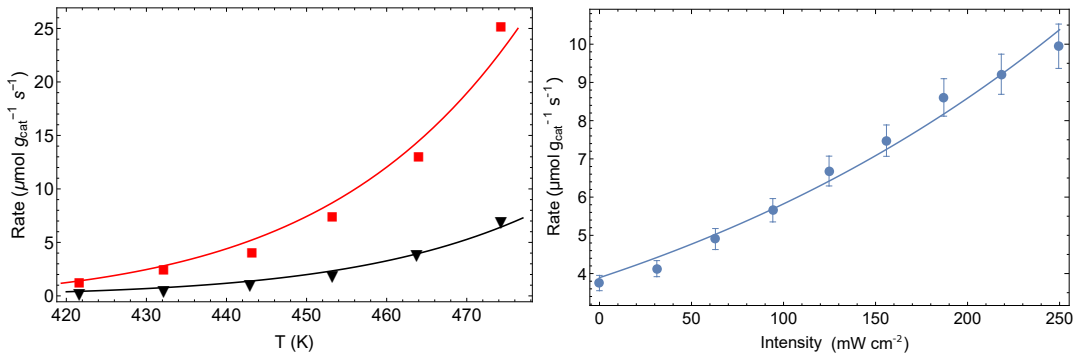


FIG. S7. (Color online) reaction rate data from Ref. [3]. Left: reaction rates in the dark (black triangles) and under illumination (red squares). Solid lines are fits to a thermal Arrhenius form, giving  $\mathcal{E}_a = 0.88\text{eV}$  and  $T - T_M \sim 20\text{K}$ . Right: reaction rates as a function of illumination intensity. Points are experimental data, and solid line is a fit to an Arrhenius form, with essentially no fit parameters (since the photothermal conversion coefficient can be extracted from the data on the left panel, see text).

#### IV. A THERMAL INTERPRETATION OF THE KINETIC ISOTOPE EFFECT OF PAPER III

In Paper III, results of a kinetic isotope effect (KIE) are presented, which they interpret as a hallmark of the “hot”-electron mechanism. In brief, this effect measures the ratio of the reaction rates associated with two different isotopes, namely,

$$KIE \equiv R_{16}/R_{18} \sim e^{-\frac{\Delta\mathcal{E}}{k_B T}},$$

directly related to the difference in the ground state energies  $\Delta\mathcal{E} \equiv \mathcal{E}_{a,18} - \mathcal{E}_{a,16}$ . Here, we show that an excellent fit to the KIE can be made using a purely thermal theory, i.e., the shifted-Arrhenius theory.

The experiment in Paper III is performed by first measuring the reaction rate ( $\text{O}_2$  dissociation in ethylene epoxidation) using the abundant isotope ( $^{16}\text{O}$ ) as a function of illumination intensity. At each illumination intensity  $I_{inc}$ , the external (i.e., measured) temperature is reduced (from an initial value of 498K) by an amount  $\Delta T_{16}$  such that the reaction rate of the  $^{16}\text{O}$  dissociation,  $R_{16}$ , remains constant. The effective temperature of the catalyst (i.e., the temperature felt by the reaction) is then  $T = 498 + a_{16}I_{inc} - \Delta T_{16}$ , where  $\Delta T_{16}$  is the change in the measured temperature from the initial measurement (performed in the dark, i.e.,  $I_{inc} = 0$ , aimed at keeping  $R_{16}$  constant),

$$R_{16} = R_0 \exp\left(-\frac{\mathcal{E}_{a,16}}{k_B(498 + a_{16}I_{inc} - \Delta T_{16})}\right) = \text{constant}. \quad (\text{S17})$$

Thus, the temperature change (which is automatically obtained using a feedback loop) is simply  $\Delta T_{16} = a_{16}I_{inc}$ . One can estimate  $a_{16}$  from Fig. 3c of Paper III, where the temperature reduction for different intensities is presented. One finds  $a_{16} \sim 120 \pm 8.4 \text{ K cm}^2/\text{W}$ .

The measurements are then repeated with the rare isotope ( $^{18}\text{O}$ ), but with the same temperature compensation used before, namely,  $\Delta T_{16}$ . The reaction rate of  $^{18}\text{O}_2$  obeys a similar formula (S17), with two differences in parameters. The first is the (slightly) different activation energies  $\mathcal{E}_{a,16}$  and  $\mathcal{E}_{a,18}$  between the two isotopes, which is the cause of the (dark) isotope effect, i.e., the difference in the reaction rates at  $I_{inc} = 0$ . The KIE was 1.09, such that the difference in the activation energies can easily be computed (not fitted), and is found to be  $\Delta\mathcal{E} = \mathcal{E}_{a,18} - \mathcal{E}_{a,16} = 0.00369\text{eV}$  (this is smaller than the measured temperature). This difference is in agreement with values than can be found in the literature.

The second difference is that the measurement can have a slightly different photo-thermal conversion coefficient  $a_{18}$ , the origin of the difference discussed below. If  $a_{18} \neq a_{16}$ , then, the adjustment of the reaction temperature  $\Delta T_{16}$  does not cancel the heating effect of the illumination for the  $^{18}\text{O}_2$  case. Simply put,  $\Delta T_{16} = a_{16}I_{inc} \neq a_{18}I_{inc}$ .

Thus, when the intensity is increased, the rate  $R_{16}$  remains unchanged, while the rate  $R_{18}$  changes because of heating, and their ratio is the measured KIE. Once can evaluate it

by using the Arrhenius formula.

$$\begin{aligned}
 R_{18} &= R_0 \exp\left(-\frac{\mathcal{E}_{a,18}}{k_B(498 + a_{18}I_{inc} - \Delta T)}\right) \\
 &= R_0 \exp\left(-\frac{\mathcal{E}_{a,18}}{k_B(498 + (a_{18} - a_{16})I_{inc})}\right).
 \end{aligned}
 \tag{S18}$$

The measured KIE is then found by combining Eqs. (S17) and (S18),

$$KIE \equiv R_{16}/R_{18} = \exp\left(\frac{\mathcal{E}_{a,16} + \Delta\mathcal{E}}{k_B T + (a_{18} - a_{16})I_{inc}} - \frac{\mathcal{E}_{a,16}}{k_B T}\right).
 \tag{S19}$$

Since  $\Delta\mathcal{E}$  is known from the KIE in the dark, and  $a_{16}$  is known from the fits to the data in the main text, we can now use the KIE data to find  $a_{18}$ .

In Fig. S8, we plot the KIE data taken from Paper III (blue points, including the error bars). On top of that, we show a fit based on the theoretical KIE (solid red line; Eq.(S19)). To obtain the fit of Fig. S8, it turns out that one only needs a small change in the photothermal conversion coefficient, to reproduce the the experimental data; the KIE can be fitted very well with  $a_{18} = 113 \text{ K cm}^2/\text{W}$ . The difference between  $a_{18}$  and  $a_{16}$  is only  $\sim 5.5\%$ . Such a difference can arise from a variety of differences between the experiments, for instance the gas density or velocity, sample size, thermal conductivity, sample degradation, etc.. Either way, 5% is far less than the variations in the photothermal conversion coefficient observed between different figures in Paper III.

## V. THE EFFECT OF CONVECTION ON THE PELLET TEMPERATURE

In the calculations of the previous sections, we assumed that the temperature distribution in the environment is determined just by heat diffusion. However, in references [1, 2, 21, 22], it was attempted to remove some of the heat generated in the NPs by gas flows in the reaction chamber via convection. The movement and temperature of the gas should be rigorously described by the continuity equations for mass, momentum (Navier-Stokes equations) and energy [23]. However, due to the large domain size, unknown parameters and geometry, such numerical calculation could be time-consuming and computational costly or even unfeasible.

Instead, let us estimate the heat power transferred via convection by assuming that it satisfies Newton's Law of cooling [23], i.e.,

$$q_c = h_c \cdot A \cdot \Delta T,
 \tag{S20}$$

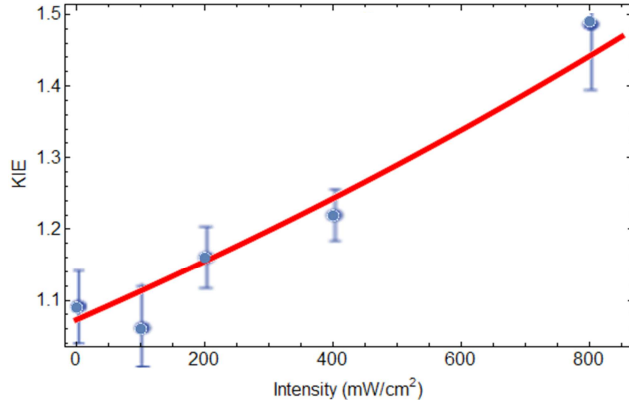


FIG. S8. The kinetic isotope effect data of Paper III (blue points) and the fit to an Arrhenius theory (solid red line). Obtaining this fit requires a single fitting parameter, which is the photo-thermal conversion factor for the rare isotope measurement. The data can be fitted to excellent degree with a very small difference in the photo-thermal conversion coefficient, around 5.5%.

where  $q_c$  is the heat power transferred via convection,  $h_c$  is the convective heat transfer coefficient,  $A$  is the heat transfer surface area and  $\Delta T$  is the difference between the pellet surface temperature and the temperature of the gas far away from the pellet.

The convective heat transfer coefficient is usually determined empirically because it depends not only on the properties of the catalyst and the gas, but also on the flow conditions and the inner geometry of the reactor. In the following estimate, for simplicity, we set  $h_c = 22 \text{ W}/(\text{m}^2 \cdot \text{K})$  [24], the value as that of air with flow velocity of 2 m/s [24]; this value is much higher [25] than those reported in references [1, 2, 21, 22].

In particular, in reference [21, Paper I], 10 sccm of  $\text{H}_2$  and 10 sccm of  $\text{D}_2$  were flown through the chamber, the area of the top surface of the pellet was  $A \approx 16\pi \text{ mm}^2$  and the temperature difference is deduced to be  $\Delta T \approx 65 \text{ K}$  for incident laser intensity of  $2.4 \text{ W}/\text{cm}^2$  in Section III A. Thus, the heat power transferred via convection is  $\sim 0.07 \text{ W}$ , about 6% of the incident power. Similarly, in reference [22, Paper II], the photo-thermal conversion coefficient deduced in Section III A is  $\sim 5 - 10$  times larger than that of reference [21, Paper I]. Accordingly, the heat power transferred via convection is  $\sim 5 - 10$  times larger, which is

$\sim 30\%$  -  $60\%$  of the incident power. In reference [1, Paper III], 20 sccm of ethylene along with 20 sccm  $O_2$  and 60 sccm  $N_2$  were flown through the chamber, the area of the top surface of the pellet was  $A \approx 1 \text{ cm}^2$ . The temperature difference is deduced to be  $\Delta T \approx 32 \text{ K}$  for incident laser intensity of  $800 \text{ mW/cm}^2$  in Section IIIB and Supplementary Section IIA, so that the heat power transferred via convection is  $\sim 26.4 \text{ mW}$ , about  $9\%$  of the incident power. Finally, in reference [2, Paper IV], 5 sccm (100 sccm) of  $NH_3$  for the intensity range of  $1.6 \text{ W/cm}^2 - 3.2 \text{ W/cm}^2$  ( $4 \text{ W/cm}^2 - 9.6 \text{ W/cm}^2$ ) was flown through the chamber, the area of the top surface of the pellet was  $A \approx \pi \cdot 1 \text{ mm}^2$ . In this case, for an illumination intensity of  $3.2 \text{ W/cm}^2$ , the heat power transferred via convection is  $\sim 40 \text{ mW}$ , which is  $\sim 40\%$  of the incident power.

One can see that, at most, a few ten percents of the generated heat were removed by convection even for rates much higher than used in practice. Furthermore, since only the NPs within the skin depth act as heat sources and the skin depth is much shorter than the sample thickness, the temperature non-uniformity caused by the local heating is not expected to be eliminated by the convection. Our estimates that invalidate the claims on temperature uniformity in Papers I-IV, as well as more recently in [26], especially considering these claims were not based on any sort of calculation or estimate.

## VI. A DISCUSSION OF THE POTENTIAL ROLE OF NANOPARTICLE MELTING

In Papers I & III, the temperature rise measures and predicted is moderate. However, in Paper II, the fit results (which we predict to originate from the relatively low thermal conductivity of  $SiO_2$ ) lead to heating by several hundreds of degrees. In Paper IV, the high illumination intensities were employed, such that the temperature rise was much higher; the linear relation (2)-(3) between the reaction temperature and the incident intensity even predicts temperatures in excess of  $2000\text{K}$ . However, we should recall that at such high temperatures, the thermo-optic nonlinearity of the metal (and potentially of the host) causes the temperature to be much lower than the linear prediction [17, 18].

Some may claim that still, the temperatures predicted may be higher than the melting temperature of the nanoparticles. Then, a natural question is how would this affect the optical thermal and chemical properties of the samples.

First, we note that for small nanoparticles such as those employed in I-IV, NP melting may not be a well defined phenomenon. Indeed, it may not be precise to refer to the nanoparticles as being solid even at temperatures modestly above room temperature (e.g., for gold); instead they are unstable, in the sense that the atoms continuously migrate and the nanoparticle internal morphology fluctuates with time between various nearly degenerate states; these effects might depend, among other aspects, of the environment and to the best of our knowledge have not been characterized for Cu-Ru nanoparticles.

Nevertheless, let us adopt the severe assumption that the nanoparticles do undergo a well-defined phase transition, and furthermore that the melting temperature is significantly lower than the bulk melting temperature of Cu (but not of Ru, which has a far higher melting temperature). First, we must bear in mind that the temperature we extract from the experimental data is close to the maximum within the reactor. However, the calculations in Supplementary Section II (as well as measurements reported in [14, 27, 28]) show a rather significant temperature inhomogeneity inside the reactor such that the temperature of other parts of the reactor (most of its volume, in practice) are significantly lower, potentially by more than 50%.

Thus, the question we should ask ourselves is how melting of the nanoparticles in a small part of the reactor affect the observed reaction rate. Overall, we tend to say that the effect will be, at most, rather small. This conjecture relies on several arguments:

1. The antenna-reactor nanoparticles in the pellet were unstructured and perhaps fluxional even close to room temperature. Even if the melting causes shape modifications to each particle, this will have a small effect on average, and not affect the catalytic properties of the metal in any deleterious way.

2. Due to the presence of the surrounding oxide support and an inert atmosphere well in excess of the Cu vapor pressure, any such melting is not expected to lead to any significant or irreversible effects on the nanoparticles. The particles then solidify once the light is turned off.

3. Despite the above, even if we do assume that the melted layer drips off/evaporates, moves, merges with other particles etc., this will have only a slight change on the overall temperature distribution. Indeed, the absorption/heat source might become slightly distorted (its center shifted to a lower position within the layer), however, since clearly the final temperature distribution is determined primarily by the heat diffusion, the overall temperature

distribution (and therefore the reaction rate) would change only slightly. This is confirmed in extensive numerical simulations we have been performing recently (not shown).

- 
- [1] Christopher, P., Xin, H., Marimuthu, A. & Linic, S. Singular characteristics and unique chemical bond activation mechanisms of photocatalytic reactions on plasmonic nanostructures. *Nat. Materials* **11**, 1044–1050 (2012).
  - [2] Zhou, L. *et al.* Quantifying hot carrier and thermal contributions in plasmonic photocatalysis. *Science* **362**, 69 (2018).
  - [3] Christopher, P., Xin, H. & Linic, S. Visible-light-enhanced catalytic oxidation reactions on plasmonic silver nanostructures. *Nature Chemistry* **3**, 467 (2011).
  - [4] The sample area is not mentioned, therefore, we assume that it is uniform and similar in size to that of the quartz window of the reaction chamber.
  - [5] Maxwell, J. *A treatise on electricity and magnetism*, vol. 1 (Clarendon Press, 1881).
  - [6] Bird, R. B., Stewart, W. E. & Lightfoot, E. N. *Transport phenomena* 2nd edition,(2002).
  - [7] Pietrak, K. & Wiśniewski, T. A review of models for effective thermal conductivity of composite materials. *J. Power Technol.* **95**, 14–24 (2014).
  - [8] Reddy, H. *et al.* Temperature-dependent optical properties of single crystalline and polycrystalline silver thin films. *ACS Photonics* **4**, 1083–1091 (2017).
  - [9] Baffou, G., Quidant, R. & de Abajo, F. J. G. Nanoscale control of optical heating in complex plasmonic systems. *ACS Nano* **4**, 709–716 (2010).
  - [10] Jackson, J. D. *Classical electrodynamics* (Wiley & Sons, 1998), 3rd edn.
  - [11] Un, I. W. & Sivan, Y. Size-dependence of the photothermal response of a single metal nanosphere. *J. Appl. Phys.* **126**, 173103 (2019).
  - [12] Baffou, G. *et al.* Photoinduced heating of nanoparticle arrays. *ACS Nano* **7**, 64786488 (2013).
  - [13] We average the temperature over the surface only because the reaction occurring within the skin depth of the pellet has the highest reaction rate due to the highest temperature and will mainly contribute to the overall increase of the reaction rate.
  - [14] Li, X., Zhang, X., Everitt, H. O. & Liu, J. Light-induced thermal gradients in ruthenium catalysts significantly enhance ammonia production. *Nano Letters* **19**, 1706–1711 (2019).
  - [15] In that respect, the illustration in IV is somewhat misleading - Ru is far more scarce than Cu.

- [16] Baffou, G. & Rigneault, H. Femtosecond-pulsed optical heating of gold nanoparticles. *Phys. Rev. B* **84**, 035415 (2011).
- [17] Sivan, Y. & Chu, S.-W. Nonlinear plasmonics at high temperatures. *Nanophotonics* **6**, 317–328 (2017).
- [18] Gurwich, I. & Sivan, Y. A metal nanosphere under intense continuous wave illumination - a unique case of non-perturbative nonlinear nanophotonics. *Phys. Rev. E* **96**, 012212 (2017).
- [19] Sivan, Y., Baraban, J., Un, I. W. & Dubi, Y. Comment on “Quantifying hot carrier and thermal contributions in plasmonic photocatalysis”. *Science* **364**, eaaw9367 (2019).
- [20] Seemala, B. *et al.* Plasmon-mediated catalytic O<sub>2</sub> dissociation on ag nanostructures: Hot electrons or near fields? *ACS Energy Letters* **4**, 1803–1809 (2019).
- [21] Mukherjee, S. *et al.* Hot electrons do the impossible: Plasmon-induced dissociation of H<sub>2</sub> on Au. *Nano Letters* **13**, 240–247 (2013).
- [22] Mukherjee, S. *et al.* Hot-electron-induced dissociation of H<sub>2</sub> on gold nanoparticles supported on SiO<sub>2</sub>. *J. Am. Chem. Soc.* **136**, 64–67 (2014).
- [23] Burmeister, L. C. *Convective heat transfer* (John Wiley & Sons, 1993).
- [24] *Engineering ToolBox* (2003). [online] Available at: [https://www.engineeringtoolbox.com/convective-heat-transfer-d\\_430.html](https://www.engineeringtoolbox.com/convective-heat-transfer-d_430.html). Accessed: 15-02-2019.
- [25] A gas velocity of 2 m/s roughly corresponds to a gas flow rate of  $\sim 4000$  sccm - 12000 sccm for chamber cross-section area of  $\sim 1$  cm<sup>2</sup>.
- [26] Rej, S. *et al.* Determining plasmonic hot electron and photothermal effects during H<sub>2</sub> evolution with TiN-Pt nanohybrids. *ACS Catalysis* **10**, 5261–5271 (2020).
- [27] Zhang, X. *et al.* Plasmon-enhanced catalysis: Distinguishing thermal and nonthermal effects. *Nano Letters* **18**, 1714–1723 (2018).
- [28] Li, H., Rivallan, M., Thibault-Starzyk, F., Traverta, A. & Meunier, F. C. Effective bulk and surface temperatures of the catalyst bed of FT-IR cells used for in situ and operando studies. *Phys. Chem. Chem. Phys.* **15**, 7321 (2013).